ADVANCED FUNCTIONAL MATERIALS
www.afm-journal.de

Electric-Driven Rotation of Silicon Nanowires and Silicon Nanowire Motors

*Xiaobin Xu, Chao Liu, Kwanoh Kim, and D. L. Fan**

In this work, the first highly controllable assembly and rotation of silicon nanowires and nanomotors in suspension are reported. Si and Si composite nanowires are fabricated with precisely controlled dimensions via colloidal assisted catalytic etching. The nanowires can be rotated with deterministic speed and chirality. The rotation speed and orientation not only depend on the applied AC electric frequency, but also on the electronic type, geometry, surface coating, as well as the electric conductance of suspension mediums. Theoretical analysis is used to understand the rotation of Si nanowires, and also the electric resistivity of Si nanowires is determined from their mechanical rotation. The Si nanowires are precisely assembled into nanomotors that can be rotated with controlled speeds and orientations at prescribed locations. This work provides a new paradigm for designing and actuating various Si-based nanoelectromechanical system (NEMS) devices, which are relevant to man-made nanomotors, nanorobots, and nanoengines.

1. Introduction

The miniaturized dimension, high speed, ultra-precision and sensitivity of micro/nano electromechanical systems (MEMS/NEMS) devices have revolutionized various research areas including sensors,[1] communication[2] and biomedical devices.[3]

Rotary micromotors that can convert rotary motion into linear motion are particularly important for further advancing MEMS technologies.[4] Currently, silicon is the most widely used material for fabrication of micromotors, not only because of its abundance in nature,[5] high crystalline quality,[5] mature micro-fabrication technologies inherited from microelectronics, and compatibility with microelectronic components,[6] but also because of its enhanced mechanical properties in strength, ductility and resistance to fatigue[7] on the nanoscale. Because of these unique properties, it is of great interest to investigate controllable rotation of nanostructures made of silicon—such as Si nanowires—and their applications in rotary micro/nanomotors.

Previously, two approaches were adopted to actuate Si-based micromotors: (1) by using complex photolithography and micromachining, electrostatically driven capacitive microcombs can engage to gears of micromotors via precisely positioned microbeams, and readily convert the linear motions of combs into clockwise (CW)/counterclockwise (CCW) rotation of micromotors;[8] (2) by sequentially applying high electric voltages (hundreds of volts) on evenly spaced stators positioned adjacent to the microrotors, micromotors can be rotated in air.[4]

However, to our knowledge, no work has been reported on the rotation of Si nanowires for applications in NEMS. Moreover, the aforementioned actuation methods either require complex motion conversion devices, such as microcombs,[8] or high voltages,[4] which make the system incompatible with aqueous environments for applications in microfluidics.

Recently, it has been shown in a scheme termed as electric tweezers that DC and AC electric fields applied to patterned electrodes can compel suspended quasi 1D entities—including metallic nanowires and carbon nanotubes—to execute precise translational and rotational motion.[9] In this work, we utilized the electric tweezers to rotate Si nanowires, investigated the fundamental physics, and assembled Si nanowires into rotary nanomotors. Si and Si composite nanowires were fabricated by colloidal-assisted-catalytic etching. By applying AC electric fields, all types of Si nanowires, including n-type, p-type, and core-shell nanowires, can be readily rotated. The speed and chirality are not only determined by the magnitude, orientation, and frequency of the electric field, but also by the electronic type, geometry, surface coating of the Si nanowires, as well as the conductivity of suspension mediums. Theoretical calculations were carried out to understand the observed rotation behaviors and also to determine the electric resistivity of nanowires from their rotation. Finally Si nanowires were integrated into nanomotors. By depositing nickel segments on the tips of Si nanowires, Si nanowires can be readily assembled and rotated on pre-patterned nanomagnets at designated positions with tunable speeds and chiralities. This research provides a new viable route for design and actuation of Si based rotary NEMS devices that are relevant to man-made nanomotors, nanorobots, and nanoengines.

X. Xu, C. Liu, Prof. D. L. Fan
Materials Science and Engineering Program
Texas Materials Institute
Department of Mechanical Engineering
The University of Texas at Austin
Austin, TX 78712, USA
E-mail: dfan@austin.utexas.edu
K. Kim, Prof. D. L. Fan
Department of Mechanical Engineering
University of Texas at Austin
Austin, Texas 78712, USA

DOI: 10.1002/adfm.201303505

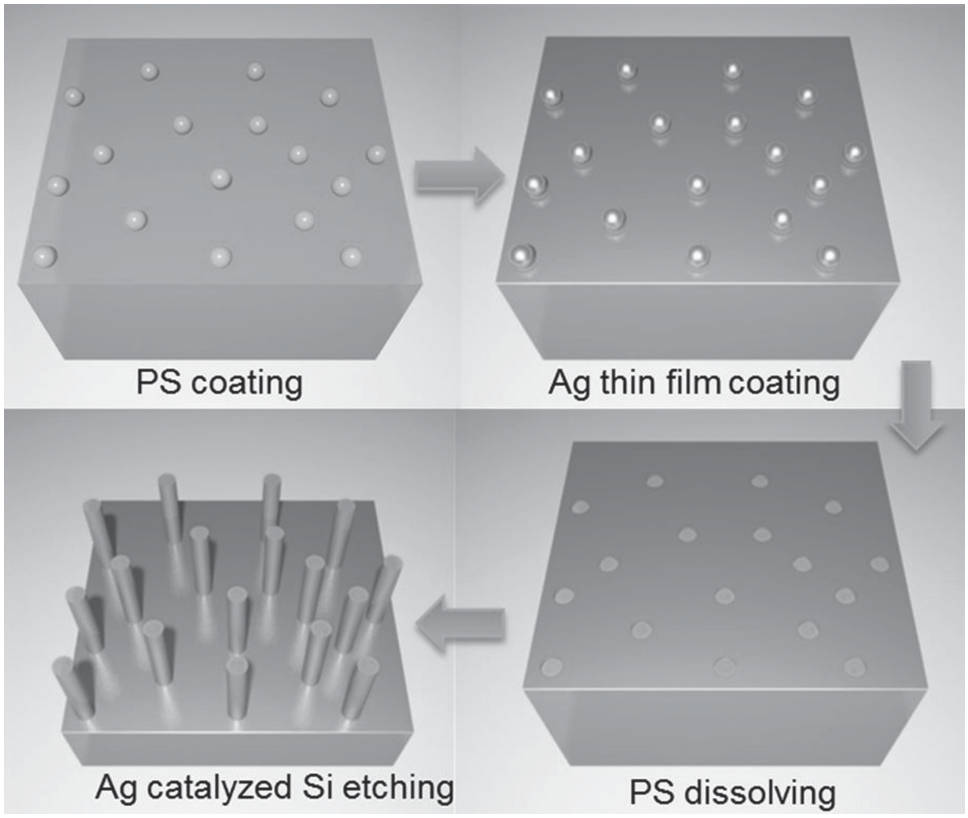

Scheme 1. Fabrication of silicon nanowires.

2. Results and Discussion

The silicon nanowires were fabricated by Ag assisted hydrofluoride etching.[10] Different from previous work, Ag catalysts were strategically patterned on the entire Si wafer with monodispersed nanoholes by using colloidal lithography.[11] Si underneath the Ag film can be readily etched while the areas not in contact with Ag remain intact. As a result, large arrays of silicon nanowires with controlled diameters and lengths can be readily formed on the wafer. The distribution of the diameters of the silicon nanowires (200 nm ± 10 nm) is much narrower compared with previous reports,[12] owing to monodispersity of polystyrene (PS) nanospheres [±5.5%, mean diameter 200 nm, **Scheme 1**, **Figure 1**c and its inset]. The detailed fabrication procedure consists of four steps as illustrated in Scheme 1 and Figure 1: first, a monolayer of monodispersed PS nanospheres (Alfa Aesar, diameter 200 nm) was electrostatically coated on a Si (100) substrate without further treatment (Figure 1a). Then a thin silver film (~50 nm) was deposited via electron-beam evaporation at a base pressure of 5×10^{-6} Torr. Next, the PS nanospheres were dissolved by toluene, exposing an array of nanoholes with controlled diameters on the Ag films (Figure 1b). Finally, the Ag patterned Si wafer was immersed in a mixture of HF (4.65 M, Acros organics) and H_2O_2 (0.25 M, J.T. Baker) for 30 min (Figure 1c). The etchant selectively removes Si underneath Ag and forms arrays of Si nanowires. The catalytic mechanism was attributed to Ag-assisted chemical reaction.[10a] In this manner, arrays of Si nanowires in the areas without Ag coverage can be formed with precisely controlled dimensions. Next, we removed the residual Ag in nitric acid solution (50%), the nanowires were cleaned, mechanically scraped, and re-dispersed in de-ionized (D.I.) water. Templated on these nanowires, various composite structures, such as SiO_2/Si, Au/Si core-shell nanowires can be readily synthesized as shown in Figure 1e, g and **Scheme 2**. The detailed fabrication processes are described in the Supporting Information (SI).

Following the nanowire synthesis, droplets of 2~10 μl Si or Si composite nanowire suspensions were placed on top of a quadruple electrode and settled for 20 s before four 90° phase-shifted AC electric voltages were applied (see **Figure 2**). This electric voltage configuration provides a uniform rotating electric field in either orientation with a controlled magnitude and frequency from 5 kHz to 1 MHz. For the convenience, the rotation chirality of the *E*-field was defined along the phase shift direction in Figure 2. An optical microscope equipped with a CCD camera was employed to record the rotation of nanowires.

Both bare and core-shell silicon nanowires can be readily rotated from 5 kHz to 1 MHz as shown in the overlapped snap shots taken every 1/15 s (Figure 2 and videos S2). The rotation angle linearly increases with time at a fixed voltage (**Figure 3**a insert), where the viscous torque instantly balances the electric torque T_e. At a fixed AC frequency, the rotation speed is proportional to V^2 (Figure 3a), consistent with other types of nanowires, such as Au, Pt, ZnO, and multiwall carbon nanotubes.[9a,9e]

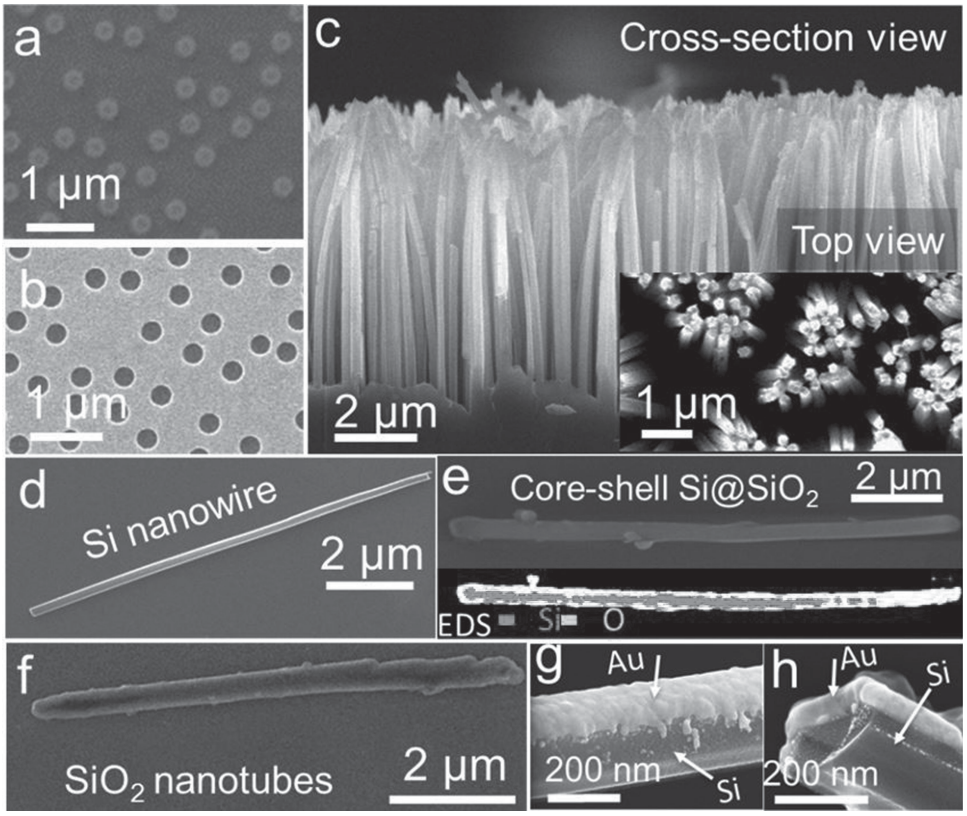

Figure 1. Scanning electron microscopy (SEM) images of (a) 200 nm-diameter PS nanospheres dispersed on a silicon wafer. (b) Ag film on a silicon wafer with 200 nm diameter holes after removal of PS nanospheres. (c) Cross-section and top view SEM images of Si nanowires fabricated by the colloidal-assisted catalytic etching method in Scheme 1. Si nanowires have uniform diameters of 200 nm. Close views of (d) a single silicon nanowire, (e) a core-shell Si/SiO_2 nanowire and its energy-dispersive X-ray spectroscopy (EDS) mapping (inset), (f) a single silica nanotube and (g,h) side and cross-sectional view of Au coated (70 nm) Si nanowires.

All Si and core-shell Si/SiO_2 nanowires switched their rotation orientations at distinct AC frequencies. The characteristics of frequency dependent rotation are determined by the surface coating, geometries of Si nanowires, as well as the electric conductance of the suspension medium. The relative electric polarization of the Si nanowires and suspension medium, represented by the imaginary part of Clausius-Mossotti factor $Im(K)$, is the key factor to understand these phenomena.

When a longitudinal nanoentity, such as a nanowire, in a liquid of permittivity ε_m rotates in an electric field $\boldsymbol{E}$, the electric torque is given as:[13a]

$$|T_e| = |p \times E| = \frac{2\pi}{3} r^2 l \varepsilon_m Im(K) E^2 \quad (1)$$

where $\boldsymbol{p}$ is the induced dipole moment of a nanowire of radius r and length l. ε_m is the permittivity of the suspension medium. The E^2 dependence counts for the V^2 dependence of Si nanowire rotation in Figure 3a.

The $Im(K)$ can be calculated as[9a,13a]

$$\mathrm{Im(K)} \approx \frac{\varepsilon_p \sigma_m - \varepsilon_m \sigma_p}{\omega\left[\left(\varepsilon_m + L\varepsilon_p - L\varepsilon_m\right)^2 + \frac{1}{\omega^2}\left(\sigma_m + L\sigma_p - L\sigma_m\right)^2\right]} \quad (2)$$

where ω is the AC frequency, σ_p, ε_p and σ_m, ε_m are conductivity and permittivity of the particle and medium, respectively, and L is the depolarization factor along the long direction of nanowires. For nanowires approximated as a prolate spheroid, L can be written in an integral form (after Laplace transform):[14]

$$L = \frac{r^2 l}{2} \int_0^\infty \frac{ds}{(s+l^2)R_s}, \quad (3)$$

where $R_s = \sqrt{\left(s+r^2\right)^2 (s+l^2)}$ and s is the elliptical coordinate.

Equations (2) and (3) show the complex dependence of $Im(K)$ on various factors including the electric properties of both the Si nanowires and suspension medium, the geometry of nanowires, as well as AC frequency (ω), However, the viscous torque (T_η) received by the rotating nanowires,[15] balances the electric torque (T_e), i.e. $T_\eta + T_e = 0$. We can readily determine $Im(K)$ from rotation speed of nanowires:

$$\Omega = -C \frac{\varepsilon_m r^2 E^2}{\eta l^2} \mathrm{Im}(K), \quad (4)$$

Where η is the viscosity, and C is a constant. Therefore, $Im(K)$ is a deterministic factor that can be used to understand and predict rotation behaviors of Si nanowires. From Equations (2) and (4), it is clear that the signs of $Im(K)$ and thus $(\varepsilon_p \sigma_m - \varepsilon_m \sigma_p)$ solely determine the rotation orientation of

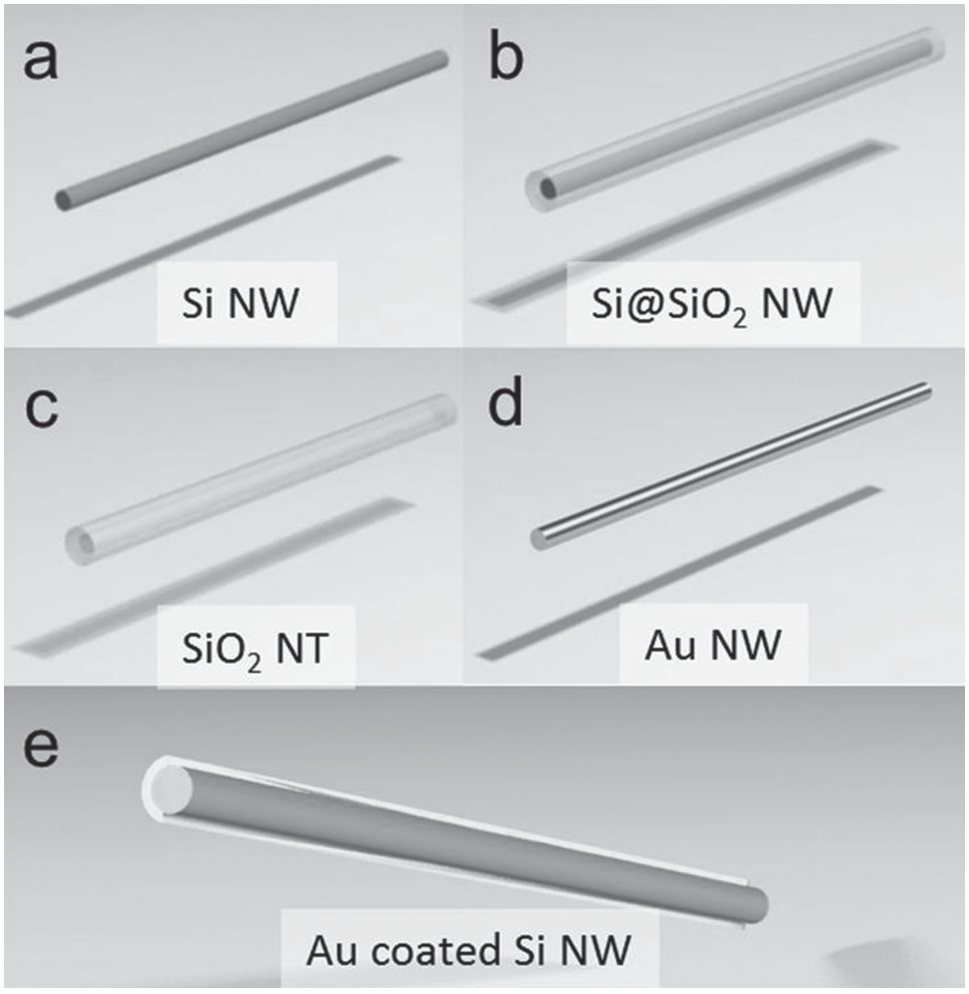

Scheme 2. Diagrams of (a) Si nanowires; (b) silica coated Si nanowires; (c) silica nanotubes; (d) Au nanowires; (e) Au coated Si nanowires.

nanowires, as the denominator of $Im(K)$ is always positive. Note that the charge relaxation time of materials is given by $\tau = \varepsilon/\sigma$. If the charge relaxation time of the nanoparticle is shorter than that of the medium $(\tau_p > \tau_m)$, then $(\varepsilon_p\sigma_m - \varepsilon_m\sigma_p) < 0$, we found the rotation of the nanowires follows the defined $\boldsymbol{E}$ fields. If the charge relaxation time of the nanoparticle is longer than that of the medium $(\tau_p < \tau_m)$, then $(\varepsilon_p\sigma_m - \varepsilon_m\sigma_p) > 0$ and the rotation of the nanowires is counterwise. When $\tau_p = \tau_m$, the nanowires do not rotate. We call the corresponding AC frequency as the cross-over frequency. The majority of the aforementioned various Si and core-shell composite Si nanowires exhibit cross-over frequencies by rotating in the same orientation with the $\boldsymbol{E}$ field before switching their rotation orientation when the frequency is increased from 5 kHz to 1 MHz. The exact cross-over frequencies, however, are distinct as listed in **Table 1**. Detailed investigation is necessary to understand these phenomena.

When rotating Si nanowires (fabricated from n-type Si wafers, 2250–3750 ohm cm), we found that the crossover frequencies, as well as the curves of rotation speed versus frequency, monotonically shift to lower frequencies with increments of nanowire lengths from 7.3 to 14.4 μm (Figure 3b). This phenomenon can be quantitatively understood from ω_p, the AC frequency at which nanowires reach the highest rotation speeds (Figure 3b). $\omega_p = (\sigma_m + L\sigma_p - L\sigma_m)/(\varepsilon_m + L\varepsilon_p - L\varepsilon_m)$ can be calculated from the first derivative of $Im(K)$ with respect to ω in Equation (2), where L can be approximated as $L \approx \left(\ln\frac{l}{r} - 1\right)\Big/\left(\frac{l}{2r}\right)^2$.[16] Considering $l/r >> 1$, we obtained $0<L<<1$ and $L \sim 1/l$. Therefore, $\omega_p \approx [\sigma_m + (\sigma_p - \sigma_m)/l]/\varepsilon_m$, which exactly agrees with our experimental observation that ω_p shifts to lower frequencies with increment of nanowire length and is linearly proportional to $1/l$ as shown in Figure 3c. From the slope of ω_p vs L [Figure S1 (a) in supporting information], which approximately equals to $(\sigma_p - \sigma_m)/\varepsilon_m$, we readily determined the resistivity of the Si nanowires as 4166 ohm cm (calculation in the supporting information). This result is at the high end of the resistivity of the Si substrates (2250–3750 ohm cm) from which the nanowires were made. The higher value found in nanowires can be attributed to a few factors: (1) the larger specific surface area and thus higher electron scattering due to the one-dimensional structure of the nanowires; (2) the thin native SiO_2 layer on the surface of nanowires, and (3) the

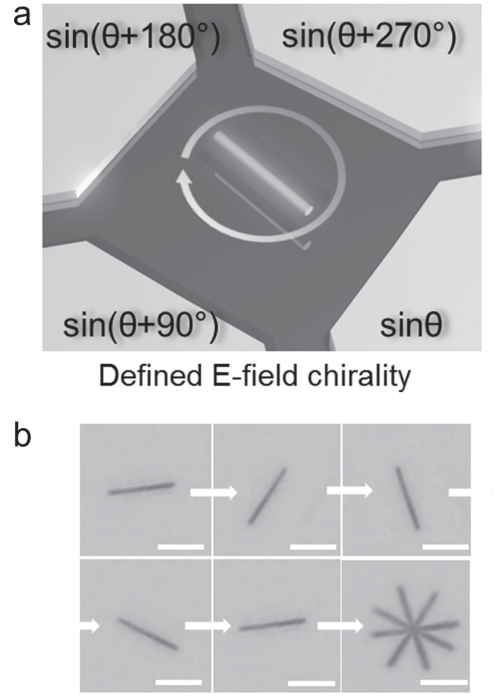

Figure 2. (a) Four 90° phase-shifted AC voltages applied to a quadruple electrode for rotation of silicon nanowires. (b) Sequential and overlapped snap shot images of a rotating Si nanowire (2250–3750 ohm cm, 14.4 μm in length) taken every 1/15 s at 15 V, 1 MHz. (Scale bar is 10 μm).

possible carrier depletion effect.[17] Therefore, by mechanically rotating nanoentities in an electric field, we readily determined their electric resistivity, which well agrees with that of the materials they are made from. This result supports the feasibility of our modeling and calculation.

The rotation behaviors of Si nanowires also depend on the electric conductivities of the suspension medium. We sequentially rotated a single Si nanowire (fabricated from n-type Si substrates, 540–840 ohm•cm) in D.I. water (2.02 μS/cm), 0.05 mM NaCl solution (7.41 μS/cm) and 0.125 mM NaCl solution (22.10 μS/cm) (video S3). As shown in **Figure 4**a, the cross-over frequencies of nanowire rotation monotonically decreased from 290 kHz to 200 kHz with increments of the electric conductivity of the suspension medium from 2.02 to 22.10 μS/cm. This result can be understood by analyzing the charge relaxation times of both the nanowires (τ_p) and suspension medium (τ_m). As mentioned earlier, at the cross-over frequency, the charge relaxation time of nanoparticles equals to that of the suspension medium ($\tau_p = \tau_m$) and nanowires do not rotate. The cross-over frequency is 290 kHz for Si nanowires in D.I. water. However, when the conductivity of the suspension medium (σ_m) is increased from 2.02 μS/cm (D.I. water) to 7.41 μS/cm and 22.10 μS/cm (0.05 mM and 0.125 mM NaCl solution, respectively), the charge relaxation time of the medium (τ_m) was substantially reduced, as $\tau_m = \varepsilon_m / \sigma_m$, while that of the Si nanowire (τ_p) remain unchanged. As a result, $\tau_p > \tau_m$ and $Im(K)>0$ as given by Equation (2). According to the aforediscussed frequency dependent study, the nanowire should rotate counter to the ***E*** field in Figure 2. The expected results exactly agree with our experimental finding that (1) nanowires in high-conductance mediums rotate counter to the ***E*** field at the crossover frequency of nanowires in low-conductance mediums (vertical grey line in Figure 4a) and (2) that the cross-over frequencies of the Si nanowire monotonically shift lower with increment of the suspension conductivity (Figure 4a).

It is known that silicon nanowires have a native oxide layer of a few nanometers which may affect the electric properties of Si nanowires. To understand how surface coating can change rotation characteristics of Si nanowires. We controllably synthesized Si/SiO_2 core-shell nanowires and Au coated Si nanowires (Figure 1 and Scheme 2). Indeed surface coating has a significant impact on rotation of Si nanowires. As shown in Figure 4b, the coating of insulating layers such as SiO_2 reduced the overall rotation speed of Si nanowires and lowered the cross-over frequency from 400 kHz to 80 kHz. (Video S4) The Au coating significantly increased the rotation speeds by 1.3–6.8 times from 5 to 50 kHz. The change of rotation characteristics is a result of the change of the overall electronic properties of Si nanowires, which depends on complex factors including the electronic properties and dimensions of cores and shells, as well as their electric interactions, i.e. electron depletion/accumulation at the interface. This is shown by the effective complex permittivity (ε_{cs}^*) modeled for a simple core-sell composite nanosphere:[13a]

$$\varepsilon_{cs}^* = \varepsilon_s \left[a^3 + 2\left(\frac{\varepsilon_c - \varepsilon_s}{\varepsilon_c + 2\varepsilon_s} \right) \right] \Big/ \left[a^3 - \left(\frac{\varepsilon_c - \varepsilon_s}{\varepsilon_c + 2\varepsilon_s} \right) \right] \quad (5)$$

where ε_c and ε_s are the permittivity of the core and shell, respectively, and a is the ratio between the outer (R_1) and inner radius (R_2).

To better understand the surface-coating effect that we observed, we prepared and rotated SiO_2 nanotubes (300 nm in inner-diameter, 600 nm in outer-diameter and 7 μm in length) and Au nanowires (300 nm in diameter, 7 μm in length) in D.I. water (The fabrication process was described in S1). It was found that the SiO_2 nanotubes always rotate counter to the orientation of Au nanowires, and Au nanowires rotate at much higher speeds (curve with open circles in Figure 4b). The countering rotation orientations of the insulating SiO_2 nanotubes and conducting Au nanowires can be attributed to their respectively lower/higher electric conductance (σ_p) and thus longer/shorter charge relaxation time (τ_p) compared to D.I. water. When SiO_2 and Au are coated on the surface of Si nanowires, the electric conductance of the composite nanowires can be much decreased/increased compared to pure Si nanowires, which results in lower/higher electric polarization of the nanowires relative to suspension medium. Therefore the rotation speed of Si/SiO_2 and Si/Au nanowires can be considerably decreased/increased compare to Si nanowires from 5 to 100 kHz as shown in Figure 4b. By the same token, the effective charge relaxation time (τ_p) of Si/SiO_2 and Au/SiO_2 core-shell nanowires can be much increased/decreased compare to Si nanowires, which lowers/increases the respective cross-over frequencies. This analysis is evidenced by the observation that the cross-over frequency of SiO_2/Si nanowires (100 kHz) is much lower than that of Si (400 kHz), and Au/Si core-shell nanowires even do not reverse rotation orientations in the frequency range that we examined (Figure 4b).

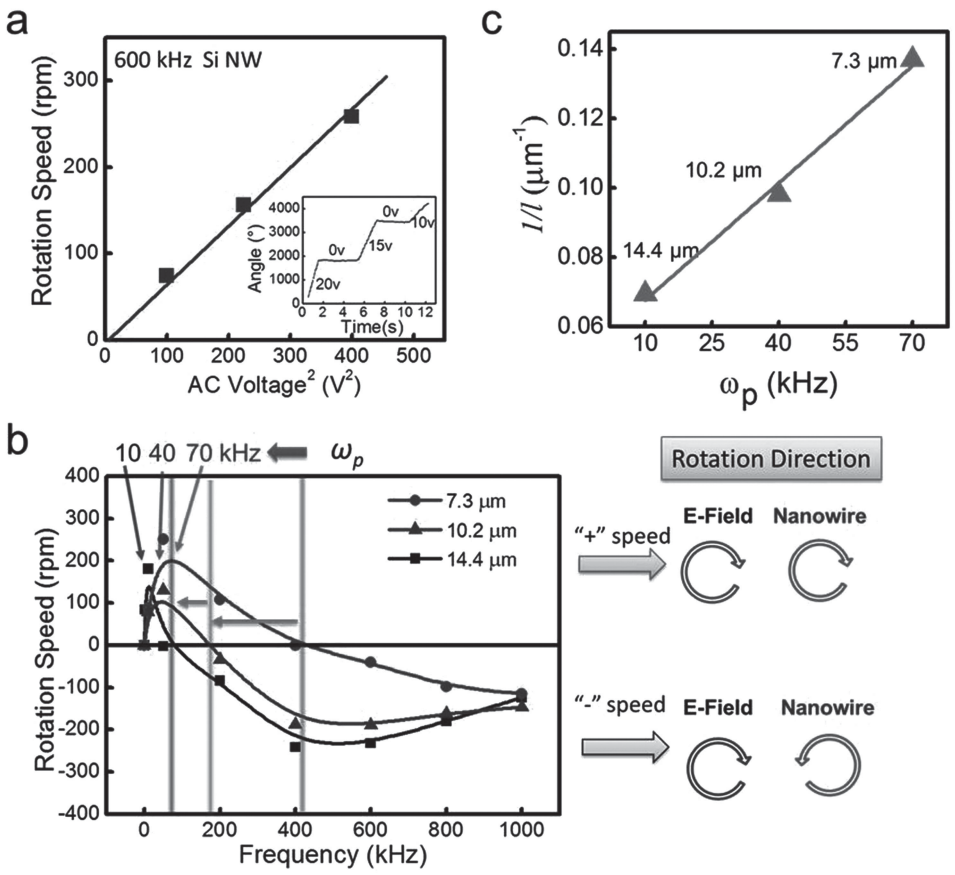

Figure 3. (a) Rotation speed of a Si nanowire (6 μm in length) linearly increases with V^2. Insert: Rotation angle is linearly proportional to time at different voltages. (b) Rotation speeds of Si nanowires (2250–3750 ohm•cm) of different lengths at 15 V. (c) Frequency (ω_p) at which a Si nanowire has the highest rotation speed shows linear dependence with 1/*l*, where *l* is the nanowire length.

Table 1. Cross-over frequencies of electric-field-driven rotation of Si nanowires.

Materials	Dimension	Suspension Medium	Cross-over frequency [kHz]
Surface coating effect on Si nanowire rotation			
Si NW (n-type)	d = 200, L = 7.3	D.I. water	430
SiO_2 nanotubes	d_{inner} = 300, d_{outer} = 600, L = 7	D.I. water	N/A
Si/SiO_2 NW	d_{Si} = 200, d_{SiO2} = 500, L = 7	D.I. water	100
Au NW	d = 300, L = 7	D.I. water	N/A
Au/Si NW	d_{Si} = 200, t_{Au} = 70, L = 7	D.I. water	200
Length-dependent Si nanowire rotation			
Si NW (n-type)	d = 200, L = 7.3	D.I. water	430
Si NW	d = 200, L = 10.2	D.I. water	170
Si NW	d = 200, L = 14.4	D.I. water	80
Si nanowire rotation in suspension of different conductivities			
Si NW(n-type)	d = 200, L = 6	D.I. water	290
Si NW(n-type)	d = 200, L = 6	NaCl 0.05 mM	270
Si NW(n-type)	d = 200, L = 6	NaCl 0.125 mM	200
Si NW(p-type)	d = 200, L = 6	D.I. water	30
d: diameter (nm), t: thickness (nm), L:length (μm)			

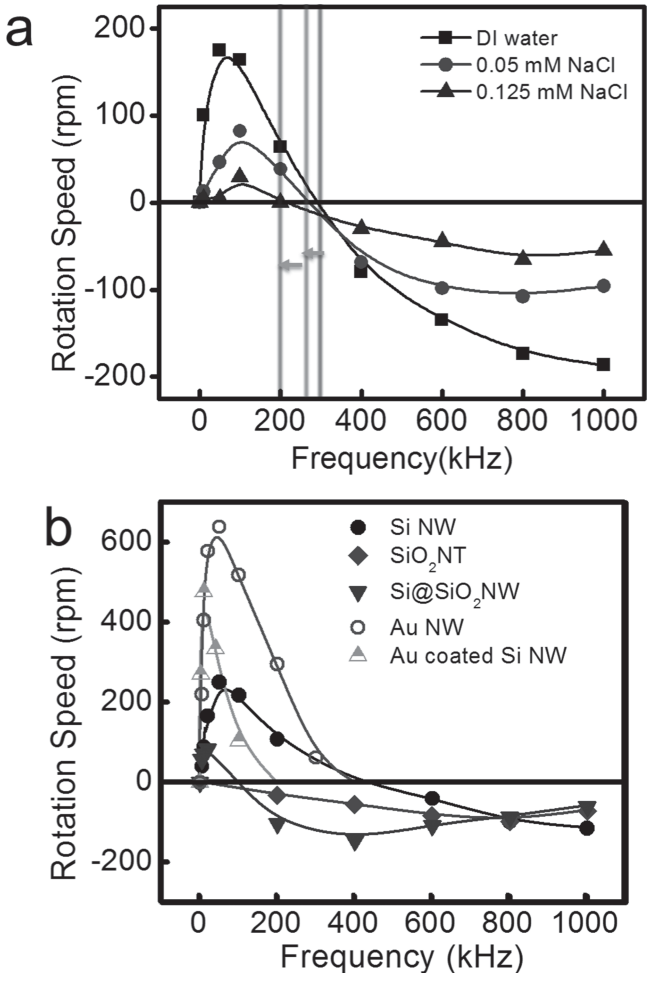

Figure 4. (a) Rotation speed versus AC frequency of a single Si nanowire in various suspension mediums, including D.I. water (2.02 μS/cm), 0.05 mM NaCl solution (7.41 μS/cm), and 0.125 mM NaCl solution (22.10 μS/cm). (b) Rotation speeds of Si, silica nanotubes, core-shell Si/SiO_2, Au, and Si/Au nanowires versus AC frequency. The nanowires are 7 μm in length.

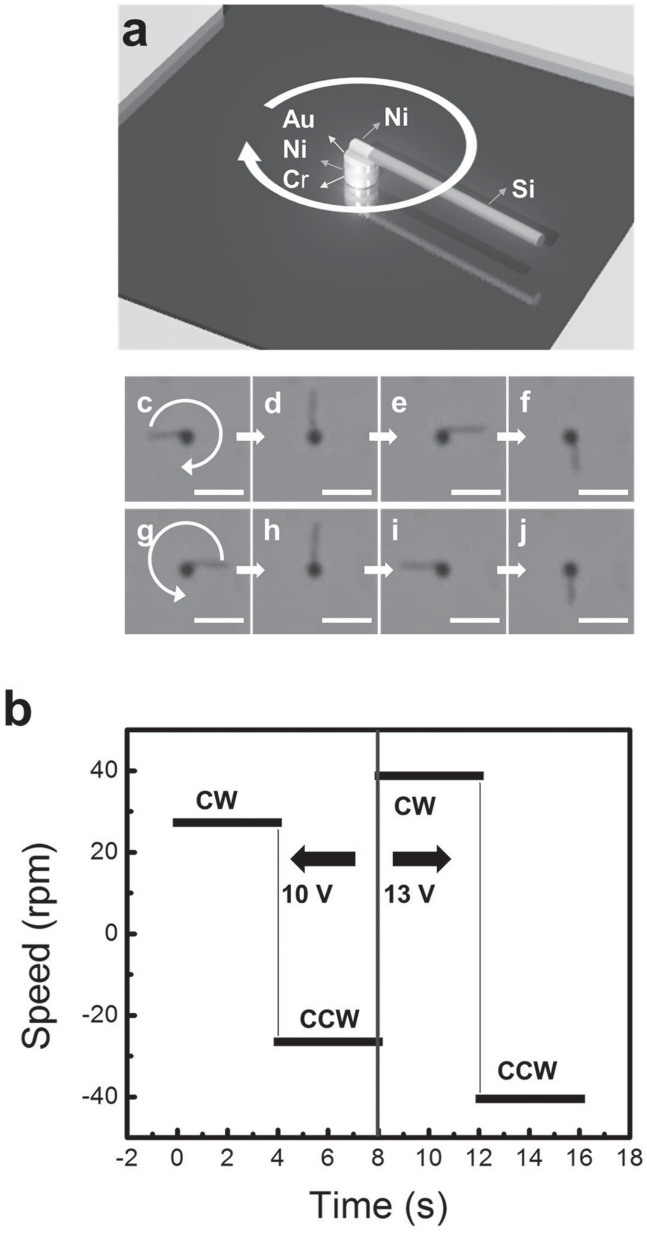

Figure 5. (a) Schematic diagram of a Si nanowire nanomotor. The magnetic disk consists of a trilayer Au/Ni/Cr thin film stack, which anchors the rotation of a Si nanowire tipped with a Ni segment. (b) The rotation speed and chirality of the nanomotor can be precisely controlled by AC electric fields (50 kHz 10–13 V). (c)-(f) the Si nanomotors can stably rotate at prescribed locations both clockwise and (g)-(j) counter-clockwise. The inset scale bar is 10 μm. The snapshots were taken every 0.4 s.

For practical applications, it is important to integrate Si nanowires into actual NEMS devices, i.e. assembling Si nanowires into nanomotors at designated locations. Recently, we successfully assembled Au-Ni-Au three segment nanowires (where Ni is magnetic) onto pre-patterned nanomagnetsusing electric tweezers[1c,9b,d,13b]—our recent invention—and studied their electric-driven rotations.[18] These Au-Ni-Au nanowires were made by electroplating into nanoporous templates. However, it is extremely difficult to electrodeposit Si nanowires and integrate magnetic segments for nanomotor assembling. To resolve this issue, we slightly altered the fabrication process of Si nanowires by evaporating a thin layer of magnetic material (Ni, 250 nm) on the tips of the Si nanowires before mechanically scraping them off from the substrate. Next, trilayer magnetic disks [Cr (6 nm)/Ni (80 nm)/Au (100 nm), 1 μm in diameter] were fabricated at the center of the quadruple electrodes by electron-beam lithography. Then, the electric-tweezers transported the Ni-tipped Si nanowires in both the X and Y directions and assembled them onto the magnetic disks. The assembling is due to the magnetic attraction between the Ni segments on the tips of Si nanowires and Ni layers in the magnetic disks. As a result, Si nanowire nanomotors can be readily made (**Figure 5**a). They rotate stably at prescribed locations with completely controlled speeds and chiralities (Figure 5b-j) (50 kHz). A real-time video can be found in the supporting information S5. The Si nanowire motors can be rotated with a speed of at least 132 rpm at 50 kHz and 20 V.

3. Conclusion

We studied controllable rotation of silicon nanowires in suspension by electric fields. Si and Si composite nanowires were fabricated with precisely-controlled dimensions using colloidal assisted catalytic etching. All Si nanowires can be rotated by electric fields. The rotation speeds and chirality are not only determined by the electric field frequency and voltage, but also by the geometry, surface coating as well as the conductivity of the suspension medium. Theoretical analysis supports our results and provides insightful understanding of Si and Si composite nanowire rotation. Electric resistivity of nanowires was determined from their mechanical rotation. By coating a nickel segment on the tips of Si nanowires, we assembled and rotated Si nanowire nanomotors at designated positions with controllable speeds and chiralities. This research provides fundamental understanding and innovative approaches for designing and actuation of various Si-nanowire based NEMS devices, which can be a big forward leap for man-made nanomotors, nanorobots, and nanoengines.

Supporting Information

Supporting Information is available from the Wiley Online Library or from the author.

Acknowledgements

X. Xu and C. Liu contributed equally to this work. We are grateful for the support of National Science Foundation CAREER Award (Grant No. CMMI 1150767), Welch Foundation (Grant No. F-1734), and UT-Austin startup package.

Received: October 12, 2013
Revised: March 18, 2014
Published online: May 7, 2014

[1] a) D. Satake, H. Ebi, N. Oku, K. Matsuda, H. Takao, M. Ashiki, M. Ishida, *Sensor Actuat. B-Chem.* **2002**, *83*, 77; b) I. M. Pryce, K. Aydin, Y. A. Kelaita, R. M. Briggs, H. A. Atwater, *Nano Lett.* **2010**, *10*, 4222; c) K. Kim, F. Q. Zhu, D. Fan, *ACS Nano* **2013**, *7*, 3476; d) H. G. Craighead, *Science* **2000**, *290*, 1532.

[2] a) D. J. Bell, T. J. Lu, N. A. Fleck, S. M. Spearing, *J. Micromech. Microeng.* **2005**, *15*, S153; b) J. Verd, A. Uranga, G. Abadal, J. L. Teva, F. Torres, J. Lopez, F. Perez-Murano, J. Esteve, N. Barniol, *IEEE Electro. Device L* **2008**, *29*, 146.

[3] a) R. X. Yan, J. H. Park, Y. Choi, C. J. Heo, S. M. Yang, L. P. Lee, P. D. Yang, *Nat. Nanotechnol.* **2012**, *7*, 191; b) W. Lee, W. Fon, B. W. Axelrod, M. L. Roukes, *Proc. Natl. Acad. Sci. USA* **2009**, *106*, 15225; c) M. Li, H. X. Tang, M. L. Roukes, *Nat. Nanotechnol.* **2007**, *2*, 114.

[4] a) Y. C. Tai, R. S. Muller, *Sens. Actuat.* **1989**, *20*, 49; b) L. G. Frechette, S. F. Nagle, R. Ghodssi, S. D. Umans, M. A. Schmidt, J. H. Lang, *4th IEEE Int. Conf. MEMS* **2001**, 290.

[5] I. H. Wilson, *Inter. J. Electro.* **1991**, *71*, 557.

[6] V. Lindroos, M. Tilli, A. Lehto, T. Motooka, *Handbook of Silicon Based MEMS Materials and Technologies*, Elsevier, Burlington, **2010**.

[7] D. M. Tang, C. L. Ren, M. S. Wang, X. L. Wei, N. Kawamoto, C. Liu, Y. Bando, M. Mitome, N. Fukata, D. Golberg, *Nano Lett.* **2012**, *12*, 1898.

[8] E. J. Garcia, J. J. Sniegowski, *Sens. Actuat. A-Phys.* **1995**, *48*, 203.

[9] a) D. L. Fan, F. Q. Zhu, X. Xu, R. C. Cammarata, C. L. Chien, *Proc. Natl. Acad. Sci. USA* **2012**, *109*, 9309; b) D. L. Fan, F. Q. Zhu, R. C. Cammarata, C. L. Chien, *Nano Today* **2011**, *6*, 339; c) D. L. Fan, Z. Z. Yin, R. Cheong, F. Q. Zhu, R. C. Cammarata, C. L. Chien, A. Levchenko, *Nat. Nanotechnol.* **2010**, *5*, 545; d) D. L. Fan, R. C. Cammarata, C. L. Chien, *Appl. Phys. Lett.* **2008**, *92*, 093115; e) D. Fan, F. Zhu, R. Cammarata, C. Chien, *Phys. Rev. Lett.* **2005**, 94.

[10] a) Z. Huang, N. Geyer, P. Werner, J. de Boor, U. Gösele, *Adv. Mater.* **2011**, *23*, 285; b) H. P. He, C. Liu, L. W. Sun, Z. Z. Ye, *Appl. Phys. Lett.* **2011**, *99*, 123106.

[11] F. Q. Zhu, D. L. Fan, X. C. Zhu, J. G. Zhu, R. C. Cammarata, C. L. Chien, *Adv. Mater.* **2004**, *16*, 2155.

[12] a) C. Chartier, S. Bastide, C. Lévy-Clément, *Electrochim. Acta* **2008**, *53*, 5509; b) Y. Qu, L. Liao, Y. Li, H. Zhang, Y. Huang, X. Duan, *Nano Lett.* **2009**, *9*, 4539; c) M. Ge, J. Rong, X. Fang, C. Zhou, *Nano Lett.* **2012**, *12*, 2318; d) K. Q. Peng, X. Wang, S. T. Lee, *Appl. Phys. Lett.* **2009**, 95.

[13] a) T. B. Jones, *Electromechanics of Particles*, Cambridge University Press, New York **1995**; b) X. B. Xu, K. Kim, H. F. Li, D. L. Fan, *Adv. Mater.* **2012**, *24*, 5457.

[14] a) R. D. Miller, T. B. Jones, *J. Biophys.* **1993**, *64*, 1588; b) R. D. Miller, *Annual Intern. Conf. IEEE Eng. In Med. Bio. Soc.* **1990**, *12*, 1513.

[15] K. Keshoju, H. Xing, L. Sun, *Appl. Phys. Lett.* **2007**, *91*, 123114.

[16] K. Asami, T. Yonezawa, *Biochim. Biophys. Acta* **1995**, *1245*, 317.

[17] a) Y. Qu, L. Liao, Y. Li, H. Zhang, Y. Huang, X. Duan, *Nano Lett.* **2009**, *9*, 4539; b) A. C. E. Chia, R. R. LaPierre, *J. Appl. Phys.* **2012**, *112*, 063705; c) Y. Qi, Z. Wang, M. Zhang, F. Yang, X. Wang, *J. Phys. Chem. C* **2013**, *117*, 25090.

[18] K. Kim, X. B. Xu, J. H. Guo, D. L. Fan, *Nature Communications* **2014**, *5*, 3632.